AAV-mediated expression of anti-tau scFvs decreases tau accumulation in a mouse model of tauopathy

Christina Ising,* Gilbert Gallardo,* Cheryl E.G. Leyns, Connie H. Wong, Hong Jiang, Floy Stewart, Lauren J. Koscal, Joseph Roh, Grace O. Robinson, Javier Remolina Serrano, and David M. Holtzman

Department of Neurology, Hope Center for Neurological Disorders, Charles F. and Joanne Knight Alzheimer's Disease Research Center, Washington University, St. Louis, MO 63110

Tauopathies are characterized by the progressive accumulation of hyperphosphorylated, aggregated forms of tau. Our laboratory has previously demonstrated that passive immunization with an anti-tau antibody, HJ8.5, decreased accumulation of pathological tau in a human P301S tau-expressing transgenic (P301S-tg) mouse model of frontotemporal dementia/tauopathy. To investigate whether the F_c domain of HJ8.5 is required for the therapeutic effect, we engineered single-chain variable fragments (scFvs) derived from HJ8.5 with variable linker lengths, all specific to human tau. Based on different binding properties, we selected two anti-tau scFvs and tested their efficacy in vivo by adeno-associated virus–mediated gene transfer to the brain of P301S-tg mice. The scFvs significantly reduced levels of hyperphosphorylated, aggregated tau in brain tissue of P301S-tg mice, associated with a decrease in detergent-soluble tau species. Interestingly, these mice showed substantial levels of scFvs in the cerebrospinal fluid without significant effects on total extracellular tau levels. Therefore, our study provides a novel strategy for anti-tau immunotherapeutics that potentially limits a detrimental proinflammatory response.

The Journal of Experimental Medicine

INTRODUCTION

Under normal conditions, tau is a highly soluble and natively unfolded microtubule-associated protein (Weingarten et al., 1975; Witman et al., 1976). However, there are several neurodegenerative diseases known as tauopathies, including progressive supranuclear palsy, corticobasal degeneration, certain forms of frontotemporal dementia, chronic traumatic encephalopathy, and Alzheimer's disease, in which hyperphosphorylated, insoluble tau accumulates inside of neurons and glia cells (Lee et al., 2001; Jeganathan et al., 2008). Interestingly, evidence suggests that accumulation of tau correlates with brain atrophy and clinical symptoms in Alzheimer's disease patients and other tauopathies (Nelson et al., 2012; Brier et al., 2016; Johnson et al., 2016). Several studies have illustrated that tau pathology appears to propagate from cell to cell in a prion-like fashion by an as-yet-unknown mechanism. Some data suggest that pathological tau escapes extracellularly, thereby entering neighboring cells transsynaptically (de Calignon et al., 2012; Lasagna-Reeves et al., 2012; Ahmed et al., 2014; Yamada et al., 2014; Clavaguera et al., 2015). If extracellular pathological tau mediates cell to cell spreading, tau binding agents that can access extracellular tau, such as anti-tau antibodies, might be a valuable tool to prevent uptake of extracellular tau into neurons or other cells to decrease spread of tau pathology. Recently, it has been shown that passive immunization with different anti-tau antibodies can have beneficial effects on tau pathology (Boutajangout et al., 2011; Chai et al., 2011; d'Abramo et al., 2013; Castillo-Carranza et al., 2015; Sankaranarayanan et al., 2015).

In line with this, we have previously developed an antibody that blocks cellular tau seeding activity very efficiently (Yanamandra et al., 2013; Holmes et al., 2014). Passive immunization with this anti-tau antibody, HJ8.5, decreased overall tau accumulation and slowed progression of the disease in a human P301S tau–expressing transgenic (P301S-tg) mouse model (Yanamandra et al., 2013, 2015). Although these results demonstrated the neuroprotective effects of a specific anti-tau immunotherapy, the mechanisms by which this and other anti-tau antibodies prevent pathological tau accumulation remain unknown. Further, treatment of brain diseases with antibodies remains a challenge in humans because only a small percentage of antibodies in the plasma are able to cross the blood–brain barrier (Yanamandra et al., 2015). Therefore, we set off to focus on understanding the mechanism by which that anti-tau antibody HJ8.5 acts, to determine whether we could improve brain delivery and, importantly, investigate the requirement of the F_c domain of the HJ8.5 antibody in decreasing tau pathology. The latter requirement was assessed by using single-chain variable fragments (scFvs) in a gene therapy approach targeting the central nervous system (CNS). ScFvs, which consist of the variable region of the heavy and the light chain connected by different peptide linkers, have

*C. Ising and G. Gallardo contributed equally to this paper.

Correspondence to David M. Holtzman: holtzman@wustl.edu

Abbreviations used: AAV, adeno-associated virus; CNS, central nervous system; CSF, cerebrospinal fluid; FA, formic acid; FRET, fluorescence resonance energy transfer; HA, hemagglutinin; htau, human tau; ICV, intracerebroventricular; ISF, interstitial fluid; scFv, single-chain variable fragment; SPR, Surface plasmon resonance.

The Rockefeller University Press $30.00
J. Exp. Med. 2017 Vol. 214 No. 5 1227–1238
https://doi.org/10.1084/jem.20162125

been shown to retain their antigen-binding specificity and, because of their small size, yield good tissue penetration and can be easily packed into an adeno-associated virus (AAV) for therapeutic delivery in the CNS (Ahmad et al., 2012).

To date, very little is known about the role of FcγRs on microglia in the neuroprotective effects of anti-tau immunotherapy. These protective effects could result either from sequestration of extracellular tau blocking cellular entrance and/or signaling or from IgG binding to FcγRs expressed on microglia that facilitate extracellular tau clearance. However, the latter may also result in a proinflammatory response and the development of adverse effects that potentially exacerbate the degenerative process (Lee et al., 2016) or even an increase in tau seeding and spreading (Asai et al., 2015). A major safety concern from early immunotherapies targeting Aβ was the development of vascular side effects that led to the discontinuation of an early clinical trial and have continued to be seen with some anti-Aβ antibodies (Senior, 2002; Nicoll et al., 2003; Orgogozo et al., 2003; Sevigny et al., 2016). Subsequently, histopathological studies implicated activation of FcγRs on microglia after immunotherapy in the development of these adverse effects (Adolfsson et al., 2012; Freeman et al., 2012).

Here, we show that anti-tau scFvs can be efficiently delivered to the brain by AAV2/8-mediated gene transfer, where they are predominantly expressed by neurons and astrocytes. The scFvs retained their antigen-binding specificity, and their expression led to a marked decrease of pathological tau accumulation in the hippocampus of P301S-tg mice. Depending on the linker used, we were able to detect secreted scFvs in the picomolar to low-nanomolar range in the cerebrospinal fluid (CSF). Interestingly, despite their effects on tau pathology, they did not affect absolute human tau (htau) levels in the CSF. Our studies provide a strategy for generating immunotherapeutics with an improved efficacy that potentially limits a proinflammatory response that may be detrimental.

RESULTS AND DISCUSSION

Length of the linker defines binding properties of anti–htau scFvs

Work over the past decades has shown that scFvs with the orientation V_L-linker-V_H show a greater binding capacity than V_H-linker-V_L constructs. Furthermore, the length of the linker influences not only efficient folding and solubility but also affinity of the scFvs (Desplancq et al., 1994; Sheikholvaezin et al., 2006). Based on these studies, we designed three anti-tau scFvs that differ only in the length of the glycine-based peptide linker that connects the variable region of the light (V_L) and the heavy chain (V_H). A secretory signal peptide was added at the N terminus and a hemagglutinin (HA) tag at the C terminus to facilitate detection (Fig. 1 A). First, we confirmed expression and secretion of all three scFvs (SC1, SC2, and SC3 scFv) in vitro. HEK293T cells were transfected with the scFv constructs, and their presence was confirmed in cell lysates as well as culture supernatants by immunoblot analysis (Fig. 1 B, bottom). To determine whether they retained their ability to bind to tau, the culture supernatant was mixed with recombinant htau, and coimmunoprecipitation was performed. Immunoblot analysis confirmed binding of the scFvs to htau (Fig. 1 B, top). To determine the specificity of anti-tau scFvs, brain lysates from P301S-tg mice and nontransgenic controls were subjected to immunoblotting analysis using purified scFvs. Notably, immunoblotting for htau revealed that all three scFvs effectively immunoreacted with htau and not mouse tau (Fig. 1 C). Additionally, surface plasmon resonance (SPR) measurements with immobilized htau revealed varying binding constants (K_D) for all three scFvs, with SC1 scFv displaying the lowest and SC2 scFv the highest K_D (Fig. 1 D). Collectively, these analyses validated that our anti-tau scFvs retain biological activity that is specific for htau, with different binding affinities.

Functional anti-tau scFvs can be expressed in the brain in vivo by AAV-mediated gene transfer

Based on our SPR data (Fig. 1 D), we decided to test the scFv with the slowest dissociation rate (SC1 scFv) and that with the fastest association rate (SC3 scFv) in vivo. Therefore, the scFvs were packaged into AAV2/8 and delivered at postnatal day 0 (P0) by bilateral intracerebroventricular (ICV) injections. Immunohistological staining with an anti-HA antibody revealed widespread expression of the scFvs throughout the brain at 3 mo after injection (Fig. 2 A). In line with a previous study (Chakrabarty et al., 2013), costaining with a neuronal (NeuN; Fig. 2 B), astrocytic (GFAP; Fig. 2 C), or microglial (Iba1; Fig. 2 D) marker revealed expression mostly in neurons and astrocytes, but rarely microglia. Furthermore, coimmunoprecipitation from brain lysates of AAV-injected P301S-tg mice showed that the scFvs retain their biological activity to bind htau (Fig. 2 E). In addition to expression in the brain, we detected scFvs in liver, heart, lung, and muscle samples of these mice (Fig. 2 F), showing that the AAV expression is not restricted to the brain despite ICV injections. However, we did not observe any gross changes in tissue morphology in 16-wk-old mice as assessed by hematoxylin and eosin staining (not depicted). Furthermore, immunoblot analysis failed to detect any scFvs in plasma samples (Fig. 2, G and H), most likely because of the short half-life of scFvs in plasma. Thus, AAVs can be used to express scFvs in the brain while retaining scFv function.

SC1 and SC3 scFvs affect soluble tau levels and decrease p-tau staining in specific hippocampal regions in aged P301S-tg mice

After validating expression of the scFvs and confirming their binding capabilities to htau, we aged AAV2/8 scFv-injected P301S-tg mice to 9 mo to investigate effects on tau pathology. P301S-tg mice begin to develop tau pathology at 5–6 mo, and it is robust by 9 mo of age. As a control, we injected mice with an AAV2/8 expressing an scFv with no binding affinity for any mouse protein. Immunoblot analysis of brain lysates

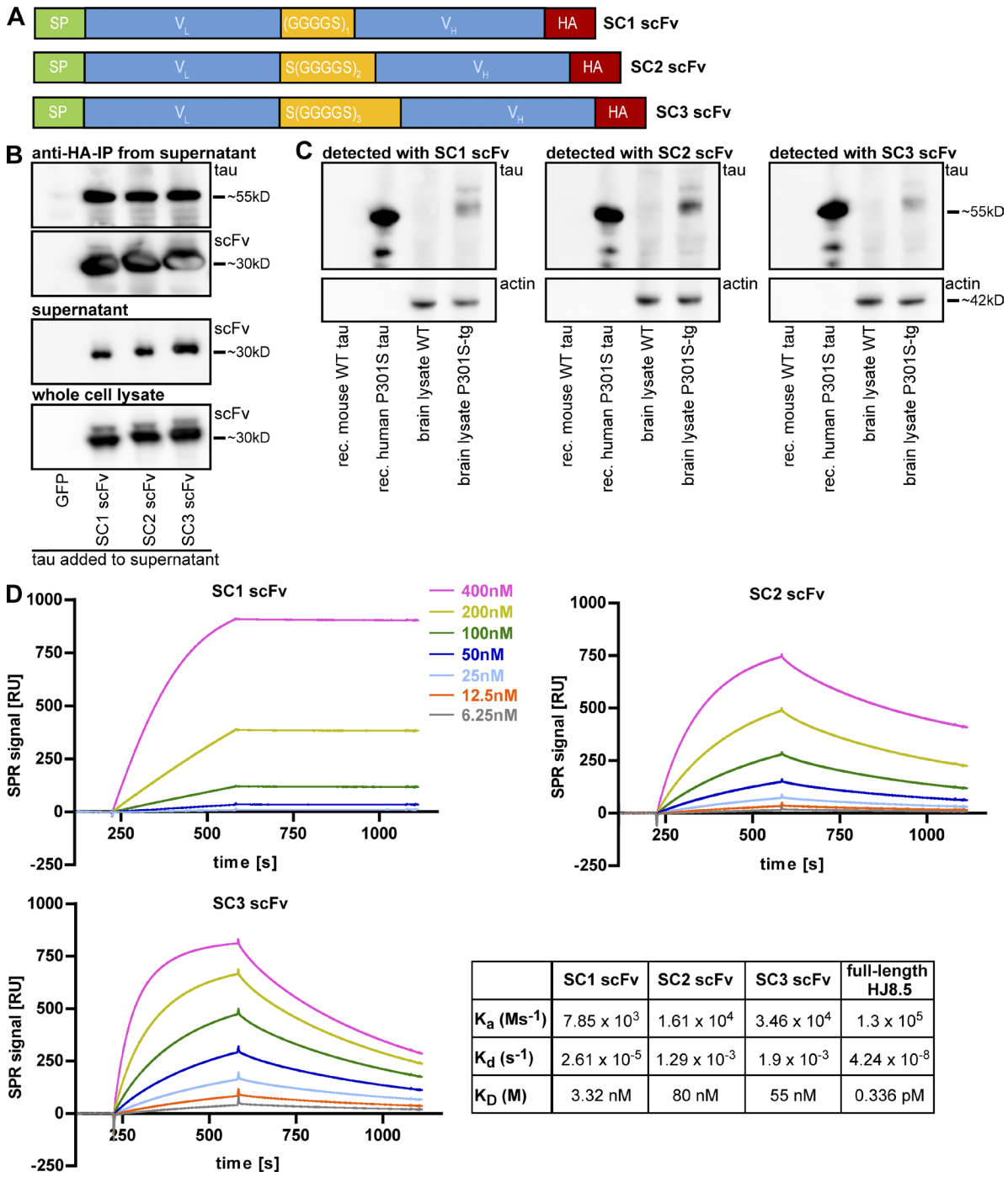

	SC1 scFv	SC2 scFv	SC3 scFv	full-length HJ8.5
K_a (Ms^{-1})	7.85 x 10^3	1.61 x 10^4	3.46 x 10^4	1.3 x 10^5
K_d (s^{-1})	2.61 x 10^{-5}	1.29 x 10^{-3}	1.9 x 10^{-3}	4.24 x 10^{-8}
K_D (M)	3.32 nM	80 nM	55 nM	0.336 pM

Figure 1. **Length of the linker defines binding properties of anti–htau–scFvs.** (A) Graphical representation of the three scFvs used. V_L, variable region of the light chain; V_H, variable region of the heavy chain; SP, secretory signal peptide; HA, HA-epitope tag. (B) Coimmunoprecipitation (IP) with an anti-HA antibody after mixing cell culture supernatants of scFv-transfected HEK 293T cells with recombinant (rec.) human P301S tau shows coprecipitation of human P301S tau with all scFv variants when analyzed by immunoblot ($n = 3$). (C) Immunoblot analysis of brain lysates from WT and P301S-tg mice as well as recombinant human P301S and mouse WT tau with scFvs used as a primary antibody shows specificity of the scFvs to htau with no detection of mtau ($n = 3$). (D) SPR measurements were performed after binding of htau to the surface and floating purified scFvs in the flow cell. Association rate (K_a), dissociation rate (K_d), and binding constant (K_D) are different for all scFv variants. RU, relative units. Values for full-length HJ8.5 in the table in D are from the original publication (Yanamandra et al., 2013). Results are representative for three independent experiments for B and C and one experiment for D.

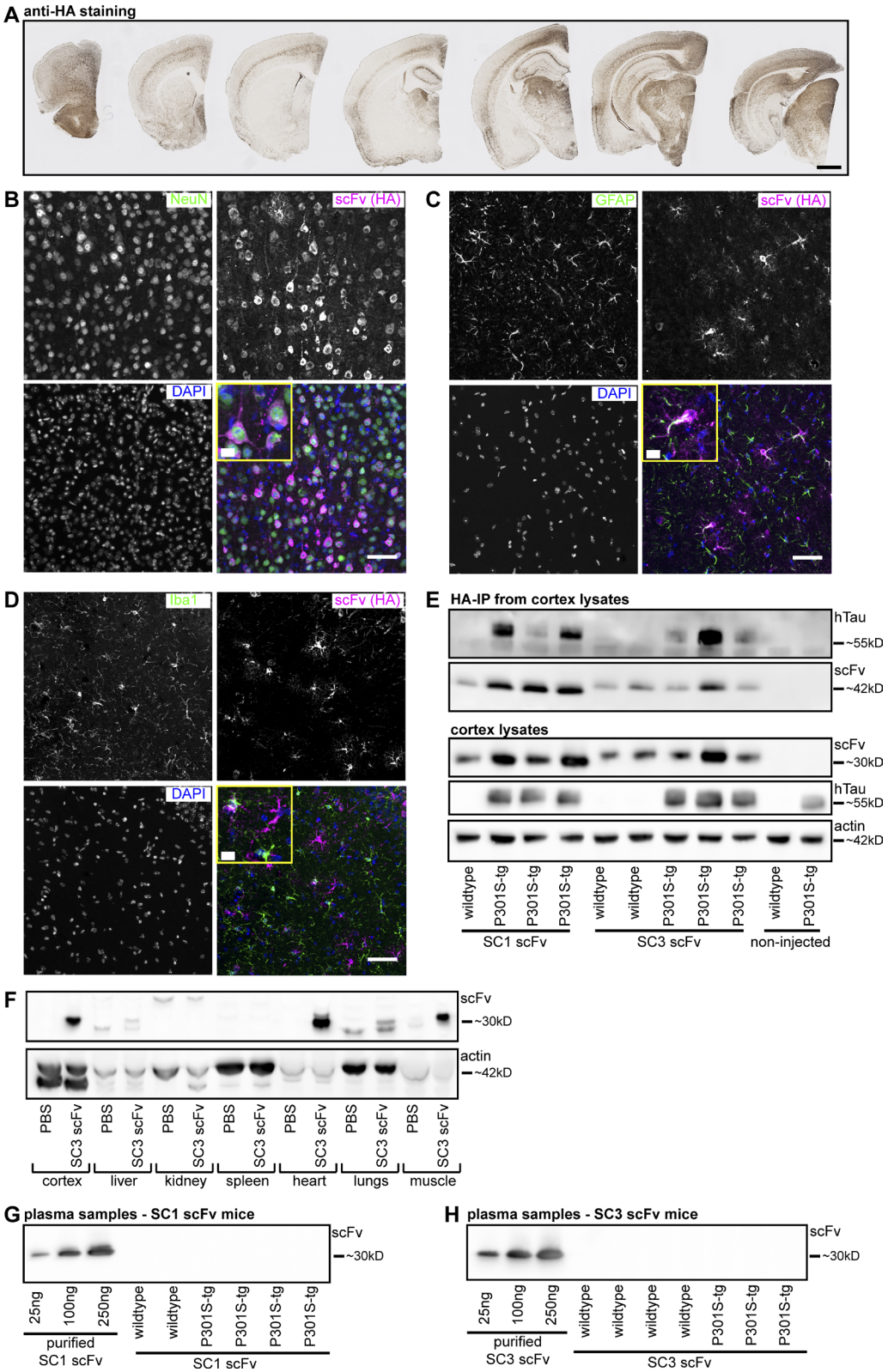

Figure 2. **Functional anti-tau scFvs can be expressed in the brain in vivo by AAV-mediated gene transfer.** (A) Immunohistochemical staining (anti-HA) of brain sections from a mouse that received an ICV injection of AAV2/8 SC3 scFv at P0 and was analyzed 3 mo later. The scFvs showed good expression throughout the brain ($n = 6$). Bar, 1 mm. (B–D) Immunofluorescence staining of brain sections from AAV2/8 scFv–injected mice with an HA anti-

confirmed expression of the scFvs in all aged mice used in this study (Fig. S1, A–C). At 9 mo of age, control scFv–treated mice displayed a substantial amount of abnormally phosphorylated htau (p-tau) in the hippocampus (stained by AT8, detecting paired helical filament tau phosphorylated at Ser202 and Thr205). Treatment with either SC1 or SC3 scFv revealed a nonsignificant trend toward lowering the levels of p-tau in assessing the entire hippocampus (Fig. 3, A and B). However, when assessing specific hippocampal subregions, there was significantly lower p-tau staining in SC1 scFv–treated mice in the CA1 cell body region (Fig. 3 C) as well as the CA1 stratum radiatum (Fig. 3 D) compared with control scFv–treated mice. Because of high variability, the effect did not quite reach statistical significance for SC3 scFv–treated mice in either region (Fig. 3, C and D). To determine soluble and insoluble htau levels, we performed sequential biochemical extractions. Hippocampus samples were first extracted in a high salt buffer (RAB buffer), before the remaining pellet was resuspended in a detergent-containing buffer (RIPA). The final pellet containing highly insoluble tau species was solubilized in a 70% formic acid (FA) solution. ELISA measurements revealed significantly higher levels of RAB-soluble htau in SC1 scFv–treated mice and the same nonsignificant trend for SC3 scFv–treated mice (Fig. 3 E). This finding was accompanied by a strong and significant decrease in htau in RIPA fractions after both treatments (Fig. 3 F). Expression of either scFv did not affect FA-soluble tau levels (Fig. 3 G). Next, we looked at levels of scFvs in RAB fractions and detected similar levels of SC1 and SC3 scFvs (Fig. S1 D). To validate binding of the scFvs to htau, we performed tau-scFv complex–specific ELISAs. These analyses demonstrated that both SC1 and SC3 scFvs are detectable in a complex with htau in hippocampal RAB fractions (Fig. S1 E). Interestingly, further analysis revealed a negative correlation for RAB-soluble htau levels with AT8 staining in the hippocampus (Fig. S2 A), whereas there was no correlation for RIPA-soluble htau (Fig. S2 B) and there was a positive correlation for insoluble htau levels (Fig. S2 C). Collectively, SC1 and SC3 scFvs decrease tau pathology as seen by p-tau staining, whereas total htau appears to be shifted from RIPA-soluble to RAB-soluble fractions.

SC1 and SC3 scFvs are detectable in CSF but do not significantly alter tau levels

Because we hypothesized a role for extracellular tau in the progression of tau pathology, we set out to determine a potential effect of the scFvs on the levels of extracellular tau. htau levels in CSF decrease over time in P301S-tg mice. Therefore, we wanted to look at time-dependent differences. First, we collected CSF from young (3–4.5 mo old) P301S-tg mice and analyzed levels of secreted scFvs by an indirect ELISA. Here, SC1 and SC3 scFvs were detectable in CSF samples of all mice, with SC3 scFv displaying a ∼40× higher level than SC1 scFv (∼263 pM for SC1 scFv vs. ∼10 nM for SC3 scFv; Fig. 4 A). Because similar levels of SC1 and SC3 scFvs are present in brain tissue (Fig. S1, D and E), this suggests a longer extracellular half-life of SC3 scFv. Analysis of htau levels in the CSF by an ELISA using a Simoa HD analyzer showed no significant differences between groups despite a trend to lower htau levels in SC3 scFv–treated mice (Fig. 4 B). In addition, we collected interstitial fluid (ISF) from the same mice by in vivo brain microdialysis and assessed htau levels by ELISA. Interestingly, we observed the same trend toward lowering htau in the ISF of SC3 scFv–treated mice (Fig. S3 A). htau levels in ISF and CSF correlated well when SC1 scFv– and SC3 scFv–treated mice were analyzed (Fig. S3 B) but showed no correlation in control scFv–treated mice (Fig. S3 C), pointing to a potentially different clearance mechanism for htau in the presence of either SC1 or SC3 scFv. To confirm binding of the scFvs to extracellular tau, we performed coimmunoprecipitation experiments from ISF samples. Immunoblot analysis confirmed binding of the scFvs to tau (Fig. S3 D).

In CSF samples of aged (9 mo old) P301S-tg mice, we found a difference in the levels of SC1 and SC3 scFvs (Fig. 4 C) similar to that seen in young mice (∼116 pM for SC1 scFv vs. ∼4 nM for SC3 scFv; Fig. 4 C). Analysis of htau levels in the CSF showed no significant differences between groups despite a trend to lower htau levels in both SC1 scFv– and SC3 scFv–treated mice (Fig. 4 D). Of note is that the concentration of htau in CSF of the young P301S-tg mice was ∼20 pM or 10× lower than the concentration of SC1. In addition to possible effects on clearance, binding of scFvs to extracellular tau could potentially influence pathology by preventing tau uptake into neurons. To test this idea, we treated neuroblastoma cells (N2a cells) and primary cortical neuronal cultures with fluorescently labeled tau in the presence and absence of scFvs and analyzed uptake by flow cytometry. Interestingly, both scFvs were able to decrease tau uptake into both cell types (Fig. S3, E and F). Furthermore, we determined the effect of the scFvs on seeding activity by using biosensor cells, which express a repeat-domain tau-YFP and -CFP construct. Seeding can be

body revealed expression of scFvs by neurons (B; NeuN) and astrocytes (C; GFAP), but rarely microglia (D; Iba1). $n = 5$ for each costaining; images represent maximum-intensity projections of *z*-stacks. Bars: (overview) 50 µm; (magnification) 10 µm. (E) Immunoblot analysis of cortex lysates (bottom) from mice injected with either AAV2/8 SC1 scFv or AAV2/8 SC3 scFv showed expression of the scFvs in all analyzed mice. Immunoprecipitation (IP) experiments (top) with an HA antibody showed coprecipitation of htau from mice that expressed the human P301S tau transgene, but not WT mice. Immunoblot is representative of two independent experiments that were performed with at least three P301S-tg mice per group. (F) Immunoblot analysis of different organs showed expression of scFvs in liver, heart, lung, and muscle lysates of mice 2.5 mo after ICV injection of AAV2/8 scFvs. Immunoblot is representative of eight independent experiments ($n = 4$ for SC1 scFv and SC3 scFv, respectively). (G and H) SC1 and SC3 scFvs were undetectable by immunoblot analysis of plasma samples from mice 2.5 mo after ICV injection of AAV2/8 scFvs ($n = 6$ for SC1 scFv and $n = 7$ for SC3 scFv).

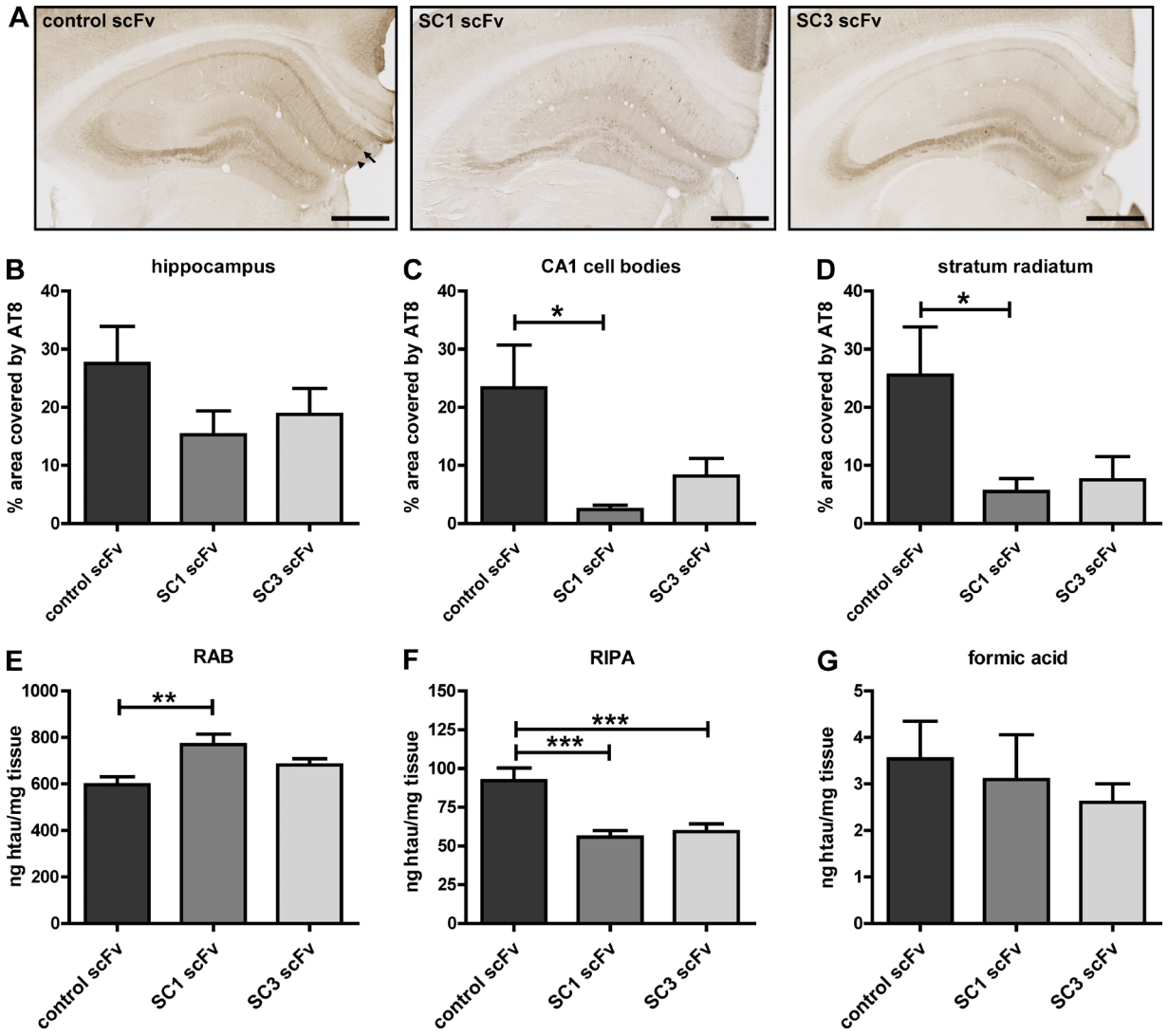

Figure 3. **SC1 and SC3 scFvs affect soluble tau levels and decrease p-tau staining in specific hippocampal regions in aged P301S-tg mice.** (A) Hippocampus of AAV2/8 scFv-injected mice after immunohistochemical staining with anti-AT8, a phospho-tau antibody. Images are representative of animals stained in one histochemical experiment (n = 17 for control scFv, n = 13 for SC1 scFv, and n = 16 for SC3 scFv). Arrow, CA1 cell body layer; arrowhead, stratum radiatum. Bars, 500 µm. (B) Quantification of percentage of area covered by AT8 showed a nonsignificant trend to lower phospho-tau in the full hippocampus (P = 0.25 by one-way ANOVA). (C and D) Quantification of percentage of area covered by AT8 showed significantly lower phospho-tau levels in CA1 cell bodies (C; *, P = 0.02 by one-way ANOVA) and the stratum radiatum (D; *, P = 0.04 by one-way ANOVA) in SC1 scFv–treated mice and nonsignificant trends for SC3 scFv–treated mice. (E–G) htau-specific ELISAs revealed significantly increased RAB-soluble tau in the hippocampus of SC1 scFv–treated mice (E; **, P = 0.006 by one-way ANOVA), decreased levels of RIPA-soluble tau in SC1 scFv– and SC3 scFv–treated mice (F; ***, P = 0.0002 by one-way ANOVA), and no difference in FA-soluble (G; P = 0.67 by one-way ANOVA) tau levels (n = 17 for control scFv, n = 14 for SC1 scFv, and n = 16 for SC3 scFv). (B–G) All graphs are means ± SEM and were analyzed by one-way ANOVA, followed by Dunnett's multiple comparison post hoc test comparing every column to control scFv: *, P < 0.05; **, P < 0.01; ***, P < 0.001.

induced by applying extracellular tau, which can then be quantified by measuring the fluorescence resonance energy transfer (FRET) signal by flow cytometry (Holmes et al., 2014). To test whether the scFvs can inhibit seeding, we immunodepleted tau from brain lysates of P301S-tg mice with the scFvs and applied those samples to the biosensor cells. Quantification of the resulting FRET signal revealed a significant decrease in seeding activity in the immunodepleted lysates compared with control-treated samples (Fig. S3 G). Thus, SC1 and SC3 scFvs are efficiently secreted but, despite substantial levels in the CSF, do not significantly affect overall total htau levels in the CSF or ISF but could potentially inhibit tau uptake and seeding.

Concluding remarks

In conclusion, we demonstrate that the length of the linker influences binding properties of scFvs to htau. ICV injection

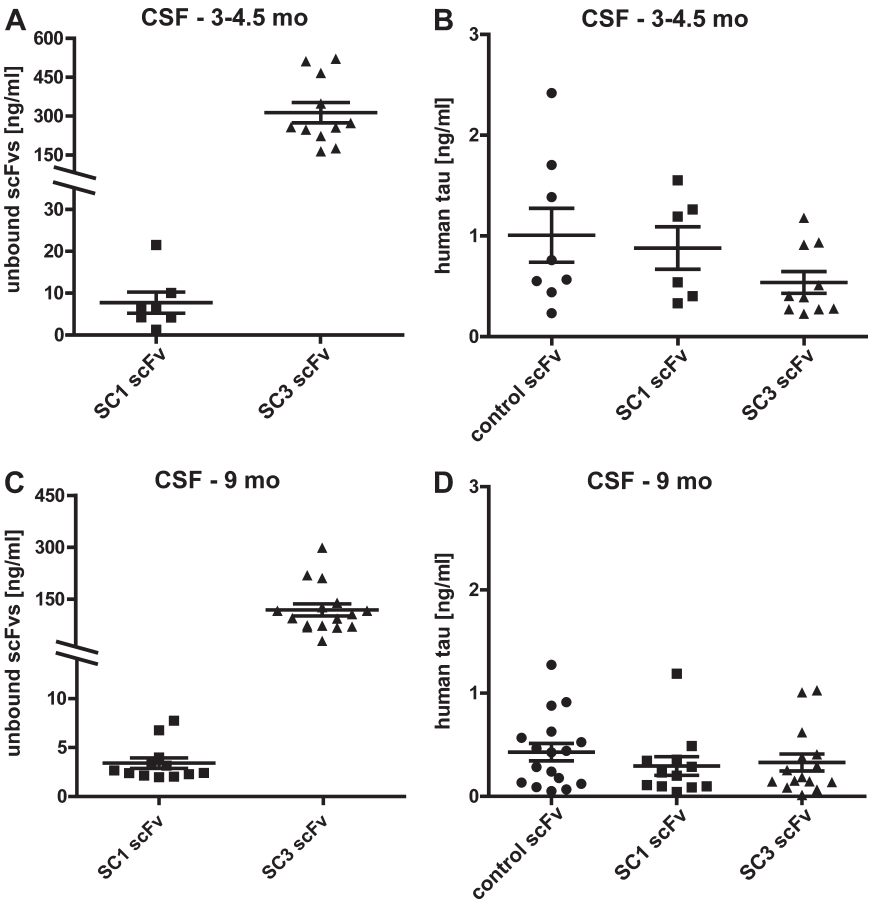

Figure 4. **SC1 and SC3 scFvs are detectable in CSF but do not significantly alter tau levels.** (A) Analysis of CSF from young (3–4.5 mo old) P301S-tg mice by ELISA revealed levels of SC1 scFvs in the low-nanomolar range (7.7 ± 2.5 ng/ml; ∼263 pM) and high levels (313 ± 39.2 ng/ml; ∼10 nM) of SC3 scFvs (n = 7 for SC1 scFv and n = 11 for SC3 scFv). (B) Analysis of htau levels in CSF samples of young P301S-tg mice by using a homebrew Simoa assay showed no significant difference between groups (n = 8 for control scFv, n = 6 for SC1 scFv, and n = 10 for SC3 scFv; P = 0.20 by one-way ANOVA). (C) ELISA measurements of scFv levels in CSF samples of 9-mo-old P301S-tg mice showed similar differences in scFv levels between SC1 scFv– and SC3 scFv–treated mice as seen in young mice (3.4 ± 0.5 ng/ml [∼116 pM] for SC1 scFv and 118.7 ± 17.4 ng/ml [∼4 nM] for SC3 scFv; n = 12 for SC1 scFv and n = 16 for SC3 scFv). (D) Analysis of htau levels in CSF samples of 9-mo-old P301S-tg mice by using a homebrew Simoa assay showed no significant difference between groups (n = 17 for control scFv, n = 12 for SC1 scFv, and n = 15 for SC3 scFv; P = 0.51 by one-way ANOVA). (A–D) All graphs represent means ± SEM.

of AAV2/8 scFvs at P0 led to widespread expression of the constructs throughout the brain, where they retained their antigen-binding capability and bound tau in the brain in vivo. Furthermore, expression of the scFvs strongly reduced p-tau and detergent-soluble tau accumulation in P301S-tg mouse hippocampus. Finally, we confirmed secretion of scFvs into the extracellular space, but intriguingly did not detect significantly altered total extracellular tau levels despite evidence of scFvs binding to extracellular tau and effects of scFvs on tau pathology.

Collectively, these results suggest that microglial-mediated tau clearance is likely not mandatory in the mechanism by which anti-tau antibodies are protective against tau accumulation. To our knowledge, this is the first study to report effects of scFv's targeting of tau to reduce tau pathology. One recent study found that p-tau staining was reduced after peripheral administration with a full-length anti–phospho-tau antibody with an effectorless F_c region mutation (Lee et al., 2016). The mechanism of the effect was not clear, as assessment of binding to tau in vivo or biochemical tau levels was not performed. Sankaranarayanan et al. (2015) recently reported reduced CSF tau levels after peripheral treatment with a full-length anti–phospho-tau antibody. These results are difficult to compare to our study because of major differences in study design. Although their group used a full-length antibody to treat rTg4510 transgenic mice, which show higher CSF tau levels in general, we used scFvs to treat P301S-tg mice. Although we did not observe an effect on total CSF tau after expression of the scFvs, we did observe binding of the scFvs to tau in the brain and ISF. This suggests that the clearance of a tau-scFv complex is likely to take on the clearance pathway of the secreted scFvs. Such binding may not alter total tau levels if the half-life of scFv-tau complexes is similar to that of unbound tau. However, such binding could alter clearance pathways of the scFv-tau complex. Clearance of scFv-tau complexes from the brain is likely to involve the brain's glymphatic system and lymphatics into CSF, neck lymph nodes, and blood as opposed to local clearance by microglia. We did observe a positive correlation between CSF htau and ISF tau, which is seen only in scFv-treated but not control mice. This suggests that anti-tau scFv–mediated clearance mechanisms act in concert with blocking tau uptake, seeding, and possibly signaling, the detailed mechanism of which can be addressed in future studies.

With regard to the development of therapeutics for tauopathies, this study could have several important implications. First, scFvs have the advantage of more efficient brain diffusion over full-length antibodies in passive immunotherapy after CNS gene transfer or direct CNS infusion (Huang et al., 2013). Second, scFvs can be cost-efficiently produced in

bacteria (Ahmad et al., 2012) whereas full-length antibodies usually have to be expressed and purified from mammalian cells. Third, lack of the F_c domain in scFvs reduces potential immunogenicity (Huang et al., 2013; Lee et al., 2016), thereby reducing the risk of inflammation-related side effects. Fourth, AAV-mediated gene transfer for therapeutic delivery could potentially be a feasible method for therapeutic delivery of scFvs. Interestingly, AAV-mediated gene transfer to the CNS is already being used successfully in clinical trials to treat several other diseases (Kantor et al., 2014). Combining this approach with the less immunogenic scFvs—which are already tested as therapeutic agents in clinical trials for other diseases (Ahmad et al., 2012)—might be a valuable tool in future therapeutic applications for brain disorders in general and tauopathies in particular.

MATERIALS AND METHODS

Animal procedures and sample collection

P301S tau transgenic mice (line PS19, purchased from The Jackson Laboratory) express the P301S human T34 isoform (1N4R) under control of the prion protein promoter. These mice are on a B6C3 background and were generated and characterized previously (Yoshiyama et al., 2007). Animal procedures were performed according to protocols approved by the Animal Studies Committee at Washington University School of Medicine. For AAV expression, pups received a bilateral ICV injection on P0 of 2 µl AAV (2.5×10^{13} vg/ml). Because of the reported high variability in tau pathology between aged male and female P301S-tg mice (Zhang et al., 2012; Yanamandra et al., 2013), we used only males for the study in which mice were aged to 9 mo, but mixed genders whenever young (3–4.5 mo old) mice were used. At time of death, mice were anesthetized and CSF was collected as described previously (DeMattos et al., 2002). Blood samples were collected in EDTA-treated tubes before cardiac perfusion with PBS/heparin. Blood samples were spun down (10 min, 2,000 *g*, 4°C), and blood plasma was collected. Brains were taken out, one hemisphere dissected and the other hemisphere immersion fixed in 4% paraformaldehyde. After 24 h, paraformaldehyde was exchanged with 30% sucrose and the brain was incubated for 48 h in this solution before it was frozen with 2-methylbutane on dry ice. Frozen brains were kept at −80°C before they were sectioned on a microtome (50-µm thickness). Floating sections were kept in 24-well plates with 30% ethylene glycol, 15% sucrose, and 0.2 M sodium phosphate at −20°C.

Antibodies

Biotinylated and unbiotinylated anti-HJ8.5 (htau-specific antibody; Yanamandra et al., 2013), anti HJ8.7 (detects htau and mouse tau [mtau]; Yanamandra et al., 2013), and anti-Tau5 (htau specific; Yanamandra et al., 2013) were used. Anti-NeuN and anti-GFAP were purchased from EMD Millipore, and anti-Iba1 was from Wako Pure Chemical Industries. Biotinylated and unbiotinylated anti–htau (clone HT7), biotinylated phospho-htau (clone AT8), and fluorescently labeled secondary antibodies were obtained from Invitrogen. Biotinylated peroxidase-coupled secondary antibodies were from Jackson ImmunoResearch Laboratories, Inc., and fluorescently labeled streptavidin was from Molecular Probes. Biotinylated anti-HA was purchased from Vector Laboratories and Bethyl Laboratories, Inc., and peroxidase-coupled anti-HA was from Roche. Anti-HA agarose beads and anti-actin were obtained from Sigma-Aldrich.

Biochemical extraction of different tau species

Frozen brain pieces were weighed, and 30 µl RAB buffer per mg of tissue added (RAB buffer = 0.75 M NaCl, 0.1 M MES, 1 mM EGTA, 0.5 mM $MgSO_4$, 2 mM DTT, and 1 mM Na_3VO_4, pH 6.8). Samples were sonicated on ice for 1 min (FB120; Thermo Fisher Scientific; 30% amplitude, 1-s intervals) before spinning them at 50,000 *g* (20 min, 4°C). The supernatant was collected (RAB fraction, contains salt-soluble tau) before adding RIPA buffer (0.15 M NaCl, 50 mM Tris, 25 mM EDTA, 1% Triton X-100, 0.5% sodium deoxycholate, and 0.5% SDS, pH 8.0) at 30 µl/mg tissue (RIPA buffer = 0.15 M NaCl, 50 mM Tris, 25 mM EDTA, 1% Triton X-100, 0.5% sodium deoxycholate, and 0.5% SDS, pH 8.0). After another round of sonication, samples were centrifuged at 50,000 *g* (20 min, 4°C). Supernatant was collected (RIPA fraction, contains detergent-soluble tau), and 10 µl of 70% FA solution per mg of tissue was added. Sonication and centrifugation and collection of supernatant (FA fraction, contains insoluble tau) were repeated. RAB and RIPA buffers were supplemented with 1× PhosSTOP and 1× cOmplete (Roche). All samples were stored at −80°C; before performing ELISA assays, FA fractions were neutralized with 1 M Tris, pH 11.

Coimmunoprecipitation

HEK293T cells were transiently transfected with Lipofectamine 2000. 48 h after transfection, supernatant was collected. After centrifugation at 1,500 *g* (5 min, room temperature), a small aliquot of each supernatant fluid was preserved and diluted with immunoblot sample buffer for immunoblot analysis (i.e., supernatant). The remaining supernatant was mixed with 10 µl anti-HA agarose beads (Sigma-Aldrich) and 1 µg recombinant human P301S tau. For coimmunoprecipitation from brain lysates, cortex pieces were homogenized in a modified RIPA buffer (50 mmol/L Tris-HCl, pH 7.4, 1% NP-40, 0.25% sodium deoxycholate, 150 mmol/L NaCl, 1 mmol/L EDTA, and protease inhibitors) and incubated on ice for 15 min. After centrifugation at 20,000 *g* (15 min, 4°C), a small aliquot of each supernatant fluid was preserved and diluted with immunoblot sample buffer for immunoblot analysis (i.e., lysate). Protein concentration was determined by BCA assay, and 100 µg protein lysate was mixed with 10 µl anti-HA agarose beads in modified RIPA buffer.

After incubation for 1 h at room temperature, the agarose beads were washed extensively with PBS, and bound

proteins were eluted by boiling the beads in immunoblot sample buffer (i.e., HA-IP).

For coimmunoprecipitation from ISF, samples were collected by in vivo brain microdialysis from SC3 scFv–injected mice. SC3 scFv concentrations were determined by ELISA, and a sample volume containing ∼800 pg SC3 scFv was used for the IPs. As a control, ISF sample buffer was mixed with purified SC3 scFvs at the same concentration. 5 µg anti-tau antibody (HJ8.7) was added to each tube, and the samples were incubated for 2 h on a rotator at 4°C. After addition of 20 µl protein G Sepharose beads (GE Healthcare), the tubes were rotated at 4°C for another 2 h. Beads were washed once with cold PBS before bound proteins were eluted by boiling the beads in immunoblot sample buffer (i.e., tau-IP). Proteins were resolved by NuPAGE Novex 4–12% Bis-Tris gels (Thermo Fisher Scientific), blotted onto nitrocellulose membranes, and visualized with enhanced chemiluminescence after incubation of the blots with the respective antibodies.

ELISA

To measure unbound scFvs, an indirect ELISA procedure was applied. Half-well 96-well plates were coated overnight at 4°C with 50 ng/ml recombinant human WT tau. After extensive washes with PBS, the wells were blocked with 4% BSA in PBS before diluted samples (sample buffer: 0.25% BSA and 300 mM Tris, pH 8.0, in PBS with protease inhibitors) were incubated overnight at 4°C. After washing, the wells were incubated with a biotinylated HA antibody (Bethyl Laboratories, Inc.) for 1.5 h. For htau-specific measurements or to detect htau–scFv complexes in brain homogenates, a sandwich ELISA was used. Plates were coated with Tau5 antibody and blocked with 4% BSA in PBS. Samples were diluted in sample buffer and, as a detector antibody, either biotinylated anti–htau (clone HT7) or biotinylated anti-HA was used. All ELI SAs were developed with super-slow TMB substrate solution (Sigma-Aldrich) before reading on a plate reader at 650 nm.

Generation and purification of scFvs

HJ8.5 monoclonal antibody was raised by immunizing tau-knockout mice with htau as described previously (Yanamandra et al., 2013). This antibody recognizes amino acids 25–30 of the full-length human 1N4R sequence (Yanamandra et al., 2013). After sequencing, the variable regions were cloned and combined in one plasmid connected by a $(GGGS)_1$-linker. A secretory signal peptide was added at the N terminus and an HA-tag at the C terminus. The different linker sequences were introduced by site-directed mutagenesis. For purification, Expi293F cells (Gibco) were grown in Expi293 Expression Medium (Gibco) to a density of 10^6 cells/ml before they were transiently transfected with Lipofectamine 2000 (Invitrogen). The scFvs were affinity-purified from supernatant 4 d later by using a HiTrap Protein L column (GE Healthcare) according to the manufacturers' instructions. After elution, the scFvs were dialyzed in PBS and concentrated with an Amicon Ultra 10K device (EMD Millipore).

Immunofluorescence

Sections were mounted on gelatin-coated slides and air-dried for 30 min. After extensive washing with PBS, sections were blocked with 5% normal goat serum in PBS with 0.1% Triton X-100. After washing, sections were incubated with primary antibodies diluted in PBS overnight at 4°C followed by three more wash steps. Fluorescently labeled secondary antibodies or streptavidin were diluted in PBS and applied to the sections. After washing, sections were coverslipped with Prolong Gold with DAPI (Invitrogen). Images were taken as a *z*-stack (one image every 1.5 µm) with a Nikon A1Rsi with a 40× oil immersion objective operated by NIS-Elements AR software version 4.30.02 (Nikon). Images were further processed with the use of ImageJ/Fiji software version 2.0.0 (National Institutes of Health) and Photoshop CS6 version 13.0.1 (Adobe Systems).

Immunohistochemistry

Sections were stained in a free-floating format in a 12-well plate. After extensive washing with TBS, sections were blocked with 0.3% hydrogen peroxide for 10 min. After washing, sections were blocked for 30 min in 3% milk in TBS and 0.25% Triton X-100 (TBS-X). The respective biotinylated primary antibody was diluted in 3% milk in TBS-X, and the sections were incubated overnight at 4°C. After washing, sections were incubated with ABC solution (VectaStain) according to the manufacturer's instructions, followed by another three wash cycles. Sections were developed in DAB solution (Sigma-Aldrich), washed, and mounted on slides. After drying overnight, sections were dehydrated in increasing ethanol concentrations followed by xylene. Slides were coverslipped with Cytoseal 60 (Thermo Fisher Scientific) and scanned on a NanoZoomer 2.0-HT system (Hamamatsu Photonics). Images were further processed and quantified with the use of ImageJ/Fiji software version 2.0.0. All areas were quantified in at least four sections (300 µm apart from each other) per mouse.

In vivo microdialysis

In vivo brain microdialysis was performed as described previously (Yamada et al., 2014). In brief, bore holes were made above the left hippocampus (AP −3.1 mm, ML −2.5 mm, DV −1.2 mm). A guide cannula (Eicom Microdialysis) was stereotactically inserted in the left hippocampus (12° angle) and cemented. After a recovery period and habituation to the Raturn sampling caging system (BASi), a 2-mm 1,000-kD MWCO cutoff AtmosLM microdialysis probe (Eicom) connected to a peristaltic push-pull pump (SciPro) was inserted through the guide cannula. As a perfusion buffer, 25% human albumin solution (Gemini Bio) was diluted to 4% with artificial CSF (1.3 mM $CaCl_2$, 1.2 mM $MgSO_4$, 3 mM KCl, 0.4 mM KH_2PO_4, 25 mM $NaHCO_3$, and 122 mM NaCl, pH 7.35). ISF samples were collected at a flow rate of either 1 or 0.5 µl/min in a refrigerated microsampler (Univentor). Analysis by ELISA was performed at the completion of each experiment.

Recombinant AAV production

All scFvs were cloned into the AAV vector under control of the chicken β-actin promoter. The rAAV2/8-scFvs used in these studies were prepared at the Hope Center Viral Vectors Core at Washington University School of Medicine.

Recombinant htau

Recombinant human P301S (1N4R) and WT tau (2N4R) were cloned into pRK172 and purified as described previously (Goedert and Jakes, 1990). Aliquots were frozen at −80°C for one-time use. For tau uptake assays, 200 µl of a 8-µM recombinant human P301S tau solution was incubated with 0.025 mg Alexa Fluor 647 NHS ester (Molecular Probes) for 1 h at room temperature before the mixture was moved to 4°C overnight. Free dye was quenched with 100 mM glycine before the sample was dialyzed in PBS.

Seeding assay

Seeding with the biosensor cells was performed as described previously (Holmes et al., 2014). In brief, htau concentration in RAB lysates from P301S-tg mice was measured by ELI SA. Lysate containing 7 nM htau was immunodepleted by incubation with 700 nM scFvs (100×) and anti-HA beads for 1 h at 4°C. After a brief centrifugation, the supernatant was diluted with PBS and mixed with Lipofectamine 2000 before adding it to the biosensor cells in a 96-well plate. Cells were incubated for 24 h before the cells were trypsinized, fixed, and resuspended in flow buffer (1× HBSS with 1% FBS and 1 mM EDTA). The number of cells with a FRET signal was analyzed on a MACSQuant VYB flow cytometer. Data analysis was performed with FlowJo Version 10 and analyzed as percentage of cells with a FRET signal within the single cell population.

Simoa assays

To measure htau in CSF samples, a Simoa homebrew assay was developed. Paramagnetic carboxylated beads (Quanterix) were activated with 0.3 mg/ml 1-ethyl-3-(3-dimethylaminopropyl) carbodiimide hydrochloride (EDC; Thermo Fisher Scientific) and coated with 0.3 mg/ml anti-HJ8.7 (binds to htau and mtau) according to the manufacturer's instructions. For detection, anti–htau (clone HT7) was biotinylated at a 40× molar ratio and used at a final concentration of 0.6 µg/ml with a SBG enzyme (Quanterix) concentration of 350 pM. All samples and standards were diluted in tau calibrator diluent (Quanterix) and run on a Simoa HD-1 analyzer (Quanterix) as a two-step assay.

Statistical analysis

All graphs represent means ± SEM. Statistical analysis was performed with GraphPad Prism 5.01 using one-way ANOVA with Dunnett's post hoc test comparing every group to the control-treated group.

SPR

SPR experiments were performed as described previously (Yanamandra et al., 2013). In brief, a Biacore sensor chip CM-5 was activated in a BIAcore 2000 SPR instrument (GE Healthcare-BIAcore) by using a 1:1 ratio of EDC and *N*-hydroxysuccinimide (NHS). Recombinant human WT tau in 10 mM sodium acetate, pH 3.5, was immobilized on the sensor chip surface with a flow rate of 5 µl/min. The remaining unbound area was blocked by 1 M ethanolamine, pH 8.5. For reference, one flow cell was activated, followed by blocking with 1 M ethanolamine. All scFvs were injected at different concentrations (6.25, 12.5, 25, 50, 100, 200, and 400 nM) in filtered, degassed 0.01 M Hepes buffer, 0.15 M NaCl, 0.005% surfactant P20, pH 7.4, at a flow rate of 10 µl/min. All samples were run in duplicate. After each run with a single antibody concentration, the surface of the chip was regenerated by using 10 mM glycine, pH 1.7. Data analysis was performed by using BIAevaluation software (GE Healthcare-BIAcore). Association (K_a) and dissociation (K_d) were calculated using Fit kinetics simultaneous K_a/K_d (global fitting) with a 1:1 (Langmuir) interaction model.

Tau uptake assay

Undifferentiated neuroblastoma cells (N2a) were split at 25,000 cells/well in a poly-L-lysine–coated 96-well plate 24 h before the start of the experiment. For uptake assays with primary cortical neurons, neurons were prepared as described previously (Beaudoin et al., 2012) and plated at 50,000 cells/well in a poly-L-lysine–coated 96-well plate. Uptake experiments were performed on 7–9 d in vitro. 20-nM Alexa Fluor 647–labeled recombinant human P301S tau (1N4R) was mixed with purified scFvs at the indicated concentrations and incubated for 30 min at room temperature in the dark. 100 µl of this mix was added to each well (technical duplicates or triplicates for each treatment), and cells were incubated for 24 h before being trypsinized and resuspended in flow buffer (1× HBSS with 1% FBS and 1 mM EDTA). The rate of tau uptake was analyzed on a MACSQuant VYB flow cytometer (20,000 cells per well analyzed for N2a cells; full well analyzed for primary cortical neurons). Data analysis was performed with FlowJo Version 10 and analyzed as relative fluorescence units.

Online supplemental material

Fig. S1 (A–C) shows immunoblots revealing expression of the scFvs in cortex lysates of all 9-mo-old P301S-tg mice analyzed in the study; Fig. S1 (D and E) shows that unbound scFvs as well as scFv-tau complexes exist in these lysates as measured by ELISA. Fig. S2 depicts correlation analysis between hippocampal AT8-staining and htau levels in RAB, RIPA, and FA fractions, demonstrating a correlation for levels of AT8 with total htau levels in RAB and FA fractions, but not RIPA fractions. Fig. S3 A shows ELISA measurements of htau levels in ISF with no significant differences between control-treated and SC1 scFv– or SC3 scFv–treated mice. Fig. S3 (B and C) depicts correlation analysis between htau levels in CSF and ISF of young mice, showing a significant correlation in treated but not control mice. Fig. S3 D shows an

immunoblot of coprecipitation experiments from ISF samples, revealing extracellular tau-scFv complexes. Fig. S3 (E and F) shows tau uptake assays with N2a neuroblastoma cells and primary cortical neuronal cultures, demonstrating significantly lower tau uptake in the presence of either SC1 or SC3 scFvs. Fig. S3 G depicts data from a seeding assay, showing that immunodepletion with SC1 or SC3 scFvs inhibits seeding activity of P301S-tg brain lysates.

ACKNOWLEDGMENTS

This work was supported by funding from the Deutsche Forschungsgemeinschaft (IS 299/1-1) to C. Ising; National Institutes of Health (NIH) grant K01 NS096719-01 and McDonnell Center for Cellular and Molecular Neurobiology grant to G. Gallardo; and from NIH grant AG04867801, Tau Consortium, the JPB Foundation, and C2N Diagnostics to D.M. Holtzman. In addition, this work was supported by The Hope Center Viral Vectors Core, The Hope Center Alafi Neuroimaging Lab, and an NIH Shared Instrumentation Grant (S10 RR027552) to Washington University School of Medicine. Immunofluorescence data acquisition with a Nikon A1Rsi microscope were performed in part through the use of the Washington University Center for Cellular Imaging.

C. Ising, G. Gallardo, C.E.G. Leyns, H. Jiang, and D.M. Holtzman are listed as inventors on a patent licensed by Washington University to C2N Diagnostics on the therapeutic use of anti-tau antibodies. D.M. Holtzman cofounded and is on the scientific advisory board of C2N Diagnostics, LLC. C2N Diagnostics, LLC has licensed certain anti-tau antibodies to AbbVie for therapeutic development. D.M. Holtzman is on the scientific advisory board of Neurophage and consults for Genentech, Eli Lilly, AbbVie, and AstraZeneca. The authors declare no additional competing financial interests.

Author contributions: C. Ising, G. Gallardo, and D.M. Holtzman conceived the study; C. Ising, G. Gallardo, C.E.G. Leyns, C.H. Wong, H. Jiang, F. Stewart, L.J. Koscal, J. Roh, G.O. Robinson, and J.Remolina Serrano carried out the experiments; C. Ising, G. Gallardo, and D.M. Holtzman designed experiments and analyzed the data; C. Ising, G. Gallardo, and D.M. Holtzman wrote the manuscript with input from all other authors. All authors approved the manuscript.

Submitted: 15 December 2016

Revised: 2 March 2017

Accepted: 3 March 2017

REFERENCES

Adolfsson, O., M. Pihlgren, N. Toni, Y. Varisco, A.L. Buccarello, K. Antoniello, S. Lohmann, K. Piorkowska, V. Gafner, J.K. Atwal, et al. 2012. An effector-reduced anti-β-amyloid (Aβ) antibody with unique aβ binding properties promotes neuroprotection and glial engulfment of Aβ. *J. Neurosci.* 32:9677–9689. http://dx.doi.org/10.1523/JNEUROSCI.4742-11.2012

Ahmad, Z.A., S.K. Yeap, A.M. Ali, W.Y. Ho, N.B.M. Alitheen, and M. Hamid. 2012. scFv antibody: Principles and clinical application. *Clin. Dev. Immunol.* 2012:980250. http://dx.doi.org/10.1155/2012/980250

Ahmed, Z., J. Cooper, T.K. Murray, K. Garn, E. McNaughton, H. Clarke, S. Parhizkar, M.A. Ward, A. Cavallini, S. Jackson, et al. 2014. A novel in vivo model of tau propagation with rapid and progressive neurofibrillary tangle pathology: The pattern of spread is determined by connectivity, not proximity. *Acta Neuropathol.* 127:667–683. http://dx.doi.org/10.1007/s00401-014-1254-6

Asai, H., S. Ikezu, S. Tsunoda, M. Medalla, J. Luebke, T. Haydar, B. Wolozin, O. Butovsky, S. Kügler, and T. Ikezu. 2015. Depletion of microglia and inhibition of exosome synthesis halt tau propagation. *Nat. Neurosci.* 18:1584–1593. http://dx.doi.org/10.1038/nn.4132

Beaudoin, G.M.J. III, S.-H. Lee, D. Singh, Y. Yuan, Y.-G. Ng, L.F. Reichardt, and J. Arikkath. 2012. Culturing pyramidal neurons from the early postnatal mouse hippocampus and cortex. *Nat. Protoc.* 7:1741–1754. http://dx.doi.org/10.1038/nprot.2012.099

Boutajangout, A., J. Ingadottir, P. Davies, and E.M. Sigurdsson. 2011. Passive immunization targeting pathological phospho-tau protein in a mouse model reduces functional decline and clears tau aggregates from the brain. *J. Neurochem.* 118:658–667. http://dx.doi.org/10.1111/j.1471-4159.2011.07337.x

Brier, M.R., B. Gordon, K. Friedrichsen, J. McCarthy, A. Stern, J. Christensen, C. Owen, P. Aldea, Y. Su, J. Hassenstab, et al. 2016. Tau and Aβ imaging, CSF measures, and cognition in Alzheimer's disease. *Sci. Transl. Med.* 8:338ra66. http://dx.doi.org/10.1126/scitranslmed.aaf2362

Castillo-Carranza, D.L., M.J. Guerrero-Muñoz, U. Sengupta, C. Hernandez, A.D.T. Barrett, K. Dineley, and R. Kayed. 2015. Tau immunotherapy modulates both pathological tau and upstream amyloid pathology in an Alzheimer's disease mouse model. *J. Neurosci.* 35:4857–4868. http://dx.doi.org/10.1523/JNEUROSCI.4989-14.2015

Chai, X., S. Wu, T.K. Murray, R. Kinley, C.V. Cella, H. Sims, N. Buckner, J. Hanmer, P. Davies, M.J. O'Neill, et al. 2011. Passive immunization with anti-Tau antibodies in two transgenic models: Reduction of Tau pathology and delay of disease progression. *J. Biol. Chem.* 286:34457–34467. http://dx.doi.org/10.1074/jbc.M111.229633

Chakrabarty, P., A. Rosario, P. Cruz, Z. Siemienski, C. Ceballos-Diaz, K. Crosby, K. Jansen, D.R. Borchelt, J.-Y. Kim, J.L. Jankowsky, et al. 2013. Capsid serotype and timing of injection determines AAV transduction in the neonatal mice brain. *PLoS One.* 8:e67680. http://dx.doi.org/10.1371/journal.pone.0067680

Clavaguera, F., J. Hench, M. Goedert, and M. Tolnay. 2015. Invited review: Prion-like transmission and spreading of tau pathology. *Neuropathol. Appl. Neurobiol.* 41:47–58. http://dx.doi.org/10.1111/nan.12197

d'Abramo, C., C.M. Acker, H.T. Jimenez, and P. Davies. 2013. Tau passive immunotherapy in mutant P301L mice: Antibody affinity versus specificity. *PLoS One.* 8:e62402. http://dx.doi.org/10.1371/journal.pone.0062402

de Calignon, A., M. Polydoro, M. Suárez-Calvet, C. William, D.H. Adamowicz, K.J. Kopeikina, R. Pitstick, N. Sahara, K.H. Ashe, G.A. Carlson, et al. 2012. Propagation of tau pathology in a model of early Alzheimer's disease. *Neuron.* 73:685–697. http://dx.doi.org/10.1016/j.neuron.2011.11.033

DeMattos, R.B., K.R. Bales, M. Parsadanian, M.A. O'Dell, E.M. Foss, S.M. Paul, and D.M. Holtzman. 2002. Plaque-associated disruption of CSF and plasma amyloid-β (Aβ) equilibrium in a mouse model of Alzheimer's disease. *J. Neurochem.* 81:229–236. http://dx.doi.org/10.1046/j.1471-4159.2002.00889.x

Desplancq, D., D.J. King, A.D. Lawson, and A. Mountain. 1994. Multimerization behaviour of single chain Fv variants for the tumour-binding antibody B72.3. *Protein Eng.* 7:1027–1033. http://dx.doi.org/10.1093/protein/7.8.1027

Freeman, G.B., T.P. Brown, K. Wallace, and K.R. Bales. 2012. Chronic administration of an aglycosylated murine antibody of ponezumab does not worsen microhemorrhages in aged Tg2576 mice. *Curr. Alzheimer Res.* 9:1059–1068. http://dx.doi.org/10.2174/156720512803569064

Goedert, M., and R. Jakes. 1990. Expression of separate isoforms of human tau protein: Correlation with the tau pattern in brain and effects on tubulin polymerization. *EMBO J.* 9:4225–4230.

Holmes, B.B., J.L. Furman, T.E. Mahan, T.R. Yamasaki, H. Mirbaha, W.C. Eades, L. Belaygorod, N.J. Cairns, D.M. Holtzman, and M.I. Diamond. 2014. Proteopathic tau seeding predicts tauopathy in vivo. *Proc. Natl. Acad. Sci. USA.* 111:E4376–E4385. http://dx.doi.org/10.1073/pnas.1411649111

Huang, L., X. Su, and H.J. Federoff. 2013. Single-chain fragment variable passive immunotherapies for neurodegenerative diseases. *Int. J. Mol. Sci.* 14:19109–19127. http://dx.doi.org/10.3390/ijms140919109

Jeganathan, S., M. von Bergen, E.-M. Mandelkow, and E. Mandelkow. 2008. The natively unfolded character of tau and its aggregation to Alzheimer-like paired helical filaments. *Biochemistry.* 47:10526–10539. http://dx.doi.org/10.1021/bi800783d

Johnson, K.A., A. Schultz, R.A. Betensky, J.A. Becker, J. Sepulcre, D. Rentz, E. Mormino, J. Chhatwal, R. Amariglio, K. Papp, et al. 2016. Tau positron emission tomographic imaging in aging and early Alzheimer disease. *Ann. Neurol.* 79:110–119. http://dx.doi.org/10.1002/ana.24546

Kantor, B., T. McCown, P. Leone, and S.J. Gray. 2014. Clinical applications involving CNS gene transfer. *Adv. Genet.* 87:71–124.

Lasagna-Reeves, C.A., D.L. Castillo-Carranza, U. Sengupta, M.J. Guerrero-Munoz, T. Kiritoshi, V. Neugebauer, G.R. Jackson, and R. Kayed. 2012. Alzheimer brain-derived tau oligomers propagate pathology from endogenous tau. *Sci. Rep.* 2:700. http://dx.doi.org/10.1038/srep00700

Lee, S.-H., C.E. Le Pichon, O. Adolfsson, V. Gafner, M. Pihlgren, H. Lin, H. Solanoy, R. Brendza, H. Ngu, O. Foreman, et al. 2016. Antibody-mediated targeting of tau in vivo does not require effector function and microglial engagement. *Cell Reports.* 16:1690–1700. http://dx.doi.org/10.1016/j.celrep.2016.06.099

Lee, V.M., M. Goedert, and J.Q. Trojanowski. 2001. Neurodegenerative tauopathies. *Annu. Rev. Neurosci.* 24:1121–1159. http://dx.doi.org/10.1146/annurev.neuro.24.1.1121

Nelson, P.T., I. Alafuzoff, E.H. Bigio, C. Bouras, H. Braak, N.J. Cairns, R.J. Castellani, B.J. Crain, P. Davies, K. Del Tredici, et al. 2012. Correlation of Alzheimer disease neuropathologic changes with cognitive status: A review of the literature. *J. Neuropathol. Exp. Neurol.* 71:362–381. http://dx.doi.org/10.1097/NEN.0b013e31825018f7

Nicoll, J.A.R., D. Wilkinson, C. Holmes, P. Steart, H. Markham, and R.O. Weller. 2003. Neuropathology of human Alzheimer disease after immunization with amyloid-β peptide: A case report. *Nat. Med.* 9:448–452. http://dx.doi.org/10.1038/nm840

Orgogozo, J.-M., S. Gilman, J.-F. Dartigues, B. Laurent, M. Puel, L.C. Kirby, P. Jouanny, B. Dubois, L. Eisner, S. Flitman, et al. 2003. Subacute meningoencephalitis in a subset of patients with AD after Aβ42 immunization. *Neurology.* 61:46–54. http://dx.doi.org/10.1212/01.WNL.0000073623.84147.A8

Sankaranarayanan, S., D.M. Barten, L. Vana, N. Devidze, L. Yang, G. Cadelina, N. Hoque, L. DeCarr, S. Keenan, A. Lin, et al. 2015. Passive immunization with phospho-tau antibodies reduces tau pathology and functional deficits in two distinct mouse tauopathy models. *PLoS One.* 10:e0125614. http://dx.doi.org/10.1371/journal.pone.0125614

Senior, K. 2002. Dosing in phase II trial of Alzheimer's vaccine suspended. *Lancet Neurol.* 1:3. http://dx.doi.org/10.1016/S1474-4422(02)00023-6

Sevigny, J., P. Chiao, T. Bussière, P.H. Weinreb, L. Williams, M. Maier, R. Dunstan, S. Salloway, T. Chen, Y. Ling, et al. 2016. The antibody aducanumab reduces Aβ plaques in Alzheimer's disease. *Nature.* 537:50–56. http://dx.doi.org/10.1038/nature19323

Sheikholvaezin, A., P. Sandström, D. Eriksson, N. Norgren, K. Riklund, and T. Stigbrand. 2006. Optimizing the generation of recombinant single-chain antibodies against placental alkaline phosphatase. *Hybrid.* 25:181–192. http://dx.doi.org/10.1089/hyb.2006.25.181

Weingarten, M.D., A.H. Lockwood, S.Y. Hwo, and M.W. Kirschner. 1975. A protein factor essential for microtubule assembly. *Proc. Natl. Acad. Sci. USA.* 72:1858–1862. http://dx.doi.org/10.1073/pnas.72.5.1858

Witman, G.B., D.W. Cleveland, M.D. Weingarten, and M.W. Kirschner. 1976. Tubulin requires tau for growth onto microtubule initiating sites. *Proc. Natl. Acad. Sci. USA.* 73:4070–4074. http://dx.doi.org/10.1073/pnas.73.11.4070

Yamada, K., J.K. Holth, F. Liao, F.R. Stewart, T.E. Mahan, H. Jiang, J.R. Cirrito, T.K. Patel, K. Hochgräfe, E.-M. Mandelkow, and D.M. Holtzman. 2014. Neuronal activity regulates extracellular tau in vivo. *J. Exp. Med.* 211:387–393. http://dx.doi.org/10.1084/jem.20131685

Yanamandra, K., N. Kfoury, H. Jiang, T.E. Mahan, S. Ma, S.E. Maloney, D.F. Wozniak, M.I. Diamond, and D.M. Holtzman. 2013. Anti-tau antibodies that block tau aggregate seeding in vitro markedly decrease pathology and improve cognition in vivo. *Neuron.* 80:402–414. http://dx.doi.org/10.1016/j.neuron.2013.07.046

Yanamandra, K., H. Jiang, T.E. Mahan, S.E. Maloney, D.F. Wozniak, M.I. Diamond, and D.M. Holtzman. 2015. Anti-tau antibody reduces insoluble tau and decreases brain atrophy. *Ann. Clin. Transl. Neurol.* 2:278–288. http://dx.doi.org/10.1002/acn3.176

Yoshiyama, Y., M. Higuchi, B. Zhang, S.-M. Huang, N. Iwata, T.C. Saido, J. Maeda, T. Suhara, J.Q. Trojanowski, and V.M.-Y. Lee. 2007. Synapse loss and microglial activation precede tangles in a P301S tauopathy mouse model. *Neuron.* 53:337–351. http://dx.doi.org/10.1016/j.neuron.2007.01.010

Zhang, B., J. Carroll, J.Q. Trojanowski, Y. Yao, M. Iba, J.S. Potuzak, A.-M.L. Hogan, S.X. Xie, C. Ballatore, A.B. Smith III, et al. 2012. The microtubule-stabilizing agent, epothilone D, reduces axonal dysfunction, neurotoxicity, cognitive deficits, and Alzheimer-like pathology in an interventional study with aged tau transgenic mice. *J. Neurosci.* 32:3601–3611. http://dx.doi.org/10.1523/JNEUROSCI.4922-11.2012